Inorganic Chemistry

including bioinorganic chemistry

February 4, 2013
Volume 52, Number 3
pubs.acs.org/IC

Broad-Band Sensitizers for Triplet–Triplet Annihilation-Based Upconversion

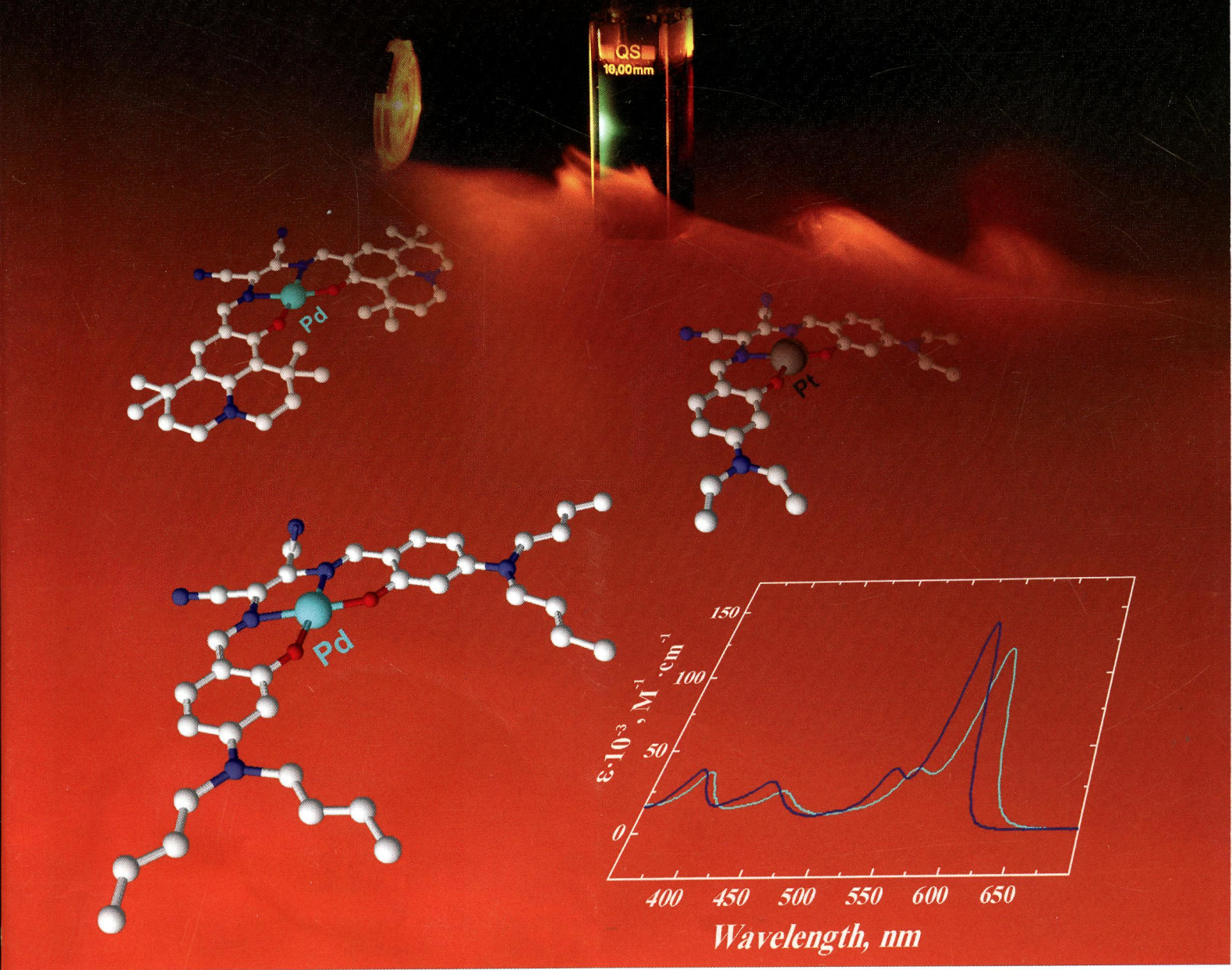

ACS Publications
MOST TRUSTED. MOST CITED. MOST READ.

www.acs.org

Inorganic Chemistry

FEBRUARY 4, 2013
VOLUME 52 ISSUE 3

INOCAJ 52(3) 1161–1666 (2013)
ISSN 0020-1669

ON THE COVER: New Pd(II) and Pt(II) complexes with donor–acceptor Schiff bases feature strong broad-band absorption in the yellow-red part of the spectrum and are efficient sensitizers of the triplet–triplet annihilation-based upconversion. See S. M. Borisov, R. Saf, R. Fischer, and I. Klimant, p 1206.

Communications

1161 S dx.doi.org/10.1021/ic301915s

A Chemosensor Built with Rhodamine Derivatives Appended to an Aromatic Platform via 1,2,3-Triazoles: Dual Detection of *Aluminum(III) and Fluoride/Acetate Ions*
Shubhra B. Maity and Parimal K. Bharadwaj*

A triazole-ring-appended rhodamine derivative (**L**) serves as a chromogenic and fluorogenic sensor for dual sensing of aluminum(III) and fluoride or acetate ions specifically in a methanolic aqueous medium.

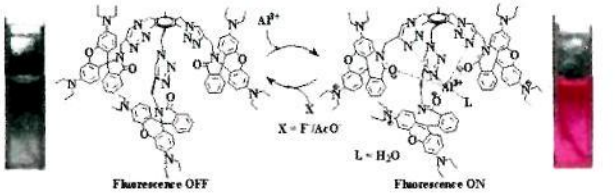

1164 S dx.doi.org/10.1021/ic3019937

A Route to Metal–Organic Frameworks through Framework Templating
Zhangwen Wei, Weigang Lu, Hai-Long Jiang, and Hong-Cai Zhou*

A microporous metal–organic framework (MOF), containing a dendritic octatopic organic linker and a Cu_2-paddlewheel structural motif, has been synthesized by using a Zn_2-paddlewheel-based MOF as a template.

1167 S dx.doi.org/10.1021/ic302175t

Lawsone Dimerization in Cobalt(III) Complexes toward the Design of New Prototypes of Bioreductive Prodrugs

Francisco L. S. Bustamante, Julia M. Metello, Frederico A. V. de Castro, Carlos B. Pinheiro, Marcos D. Pereira, and Mauricio Lanznaster*

Dimerization of lawsone occurs upon reaction with a cobalt(II) salt and the polinitrogenated ligand py_2en to produce the complex $[Co^{III}(bhnq)(py_2en)]BF_4{\cdot}H_2O$ (**1**). This complex has been investigated as a potential bioreductive prodrug, where the $bhnq^{2-}$ ligand acts as a model for cytotoxic naphthoquinones. Reactivity studies revealed the dissociation of $bhnq^{2-}$ from the complex upon reduction by ascorbic acid. Dependence of the reaction rate on the oxygen concentration suggests the occurrence of redox cycling.

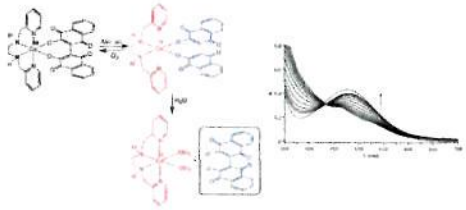

1170 S dx.doi.org/10.1021/ic302188y

Ruthenium(II) Dichloride Complexes of Chiral, Tetradentate Aminosulfoxide Ligands: Stereoisomerism and Redox-Induced Linkage Isomerism

Peter O. Atolagbe, Krista N. Taylor, Samantha E. Wood, Arnold L. Rheingold, Lenora K. Harper, Craig A. Bayse, and Tim J. Brunker*

Ruthenium(II) dichloride complexes of two tetradentate aminosulfoxide ligands have been synthesized, and all three possible geometric isomers are isolated and characterized, including an unusual *cis-α* structure with *trans* sulfur-bound sulfoxide ligands. Cyclic voltammetry studies show that only one of these isomers, *cis-β*, undergoes linkage isomerism of a sulfoxide ligand upon oxidation to ruthenium(III). An explanation based on the orientation of the HOMO, and supported by density functional theory calculations, is proposed.

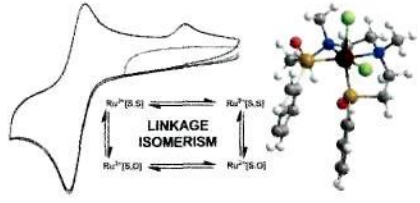

1173 S dx.doi.org/10.1021/ic3023612

Chromium(IV) Siloxide

Michael P. Marshak and Daniel G. Nocera*

The first structurally characterized homoleptic chromium(IV) siloxide complex, $Cr(OSi^tBu_2Me)_4$, has been analyzed electronically and shown to possess an unusually weak ligand field. The chromium(IV) (T_d) complex possesses ground- and excited-state topologies similar to those of the chromium(III) (O_h) complex, except the spin manifold, which is quartet/doublet for chromium(III) and triplet/singlet for chromium(IV). Unlike chromium(III) (O_h), however, no emission from the E state is observed because the extremely weak ligand field engendered by silox causes the emissive manifold to be circumvented.

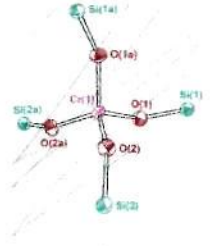

1176 S dx.doi.org/10.1021/ic3023908

2-Pyrrolyloximes in High-Nuclearity Transition-Metal Cluster Chemistry: Fe_{10} and Fe_{12}

Evangelia S. Koumousi, Anastasia Routzomani, Tu N. Nguyen, Dimosthenis P. Giannopoulos, Catherine P. Raptopoulou, Vassilis Psycharis, George Christou, and Theocharis C. Stamatatos*

The employment of 2-pyrrolyloximes in high-nuclearity transition-metal cluster chemistry has provided access to decanuclear and dodecanuclear Fe^{III} cagelike clusters bearing the anion of pyrrole-2-carboxaldehyde oxime ($praoH_2$), the simplest member of this new family of ligands.

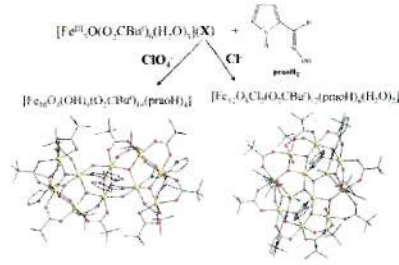

1179 S dx.doi.org/10.1021/ic302505p

Slow Magnetization Relaxation in Unprecedented $Mn^{III}_4Dy^{III}_3$ and $Mn^{III}_4Dy^{III}_5$ Clusters from the Use of *N*-Salicylidene-*o*-aminophenol

Dimitris I. Alexandropoulos, Tu N. Nguyen, Luís Cunha-Silva, Theodoros F. Zafiropoulos, Albert Escuer, George Christou, and Theocharis C. Stamatatos*

The first use of *N*-salicylidene-*o*-aminophenol in 3d/4f chemistry has led to $Mn^{III}_4Dy^{III}_5$ and $Mn^{III}_4Dy^{III}_3$ clusters with unprecedented metal topologies and stoichiometries; both compounds exhibit out-of-phase signals indicative of the slow magnetization relaxation of a single-molecule magnet.

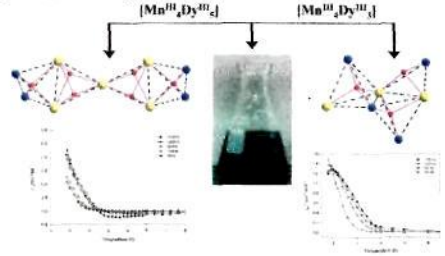

1182 S dx.doi.org/10.1021/ic302787z

Volatility and High Thermal Stability in Mid-to-Late First-Row Transition-Metal Complexes Containing 1,2,5-Triazapentadienyl Ligands

Lakmal C. Kalutarage, Mary Jane Heeg, Philip D. Martin, Mark J. Saly, David S. Kuiper, and Charles H. Winter*

The first-row transition-metal 1,2,5-triazapentadienyl complexes $M(tBuNNCHCHNR)_2$ are reported. The X-ray crystal structures of these compounds show monomeric, tetrahedral molecular geometries, and magnetic moment measurements are consistent with high-spin electronic configurations. The new complexes are volatile, exhibit high thermal stabilities, and have very useful properties for application as precursors for atomic-layer deposition.

R = tBu, NMe_2
M = Ni, Co, Fe, Mn, Cr

Articles

1185 dx.doi.org/10.1021/ic300935k

Computational Modeling of the Triplet Metal-to-Ligand Charge-Transfer Excited-State Structures of Mono-Bipyridine–Ruthenium(II) Complexes and Comparisons to their 77 K Emission Band Shapes

Richard L. Lord, Marco M. Allard, Ryan A. Thomas, Onduro S. Odongo, H. Bernhard Schlegel,* Yuan-Jang Chen, and John F. Endicott*

The medium frequency (*mf*) vibronic sideband is the dominant feature in the 77 K emission spectrum of the $[Ru(CH_3CN)_4bpy]^{2+}$ $[Ru([14]aneS_4)bpy]^{2+}$ complexes. This contrasts to the much weaker *mf* features in the spectra of $[Ru(L)_4bpy]^{n+}$ complexes with lower energy ^{3}MLCT (T_0) excited states. The calculated T_0 SOMOs for a $[Ru(NH_3)_4bpy]^{2+}$-based DFT model indicate that mixing between bpy-centered ($\pi\pi^*$) and MLCT excited states contributes to increasing the bpy distortion mode amplitudes with T_0 energy.

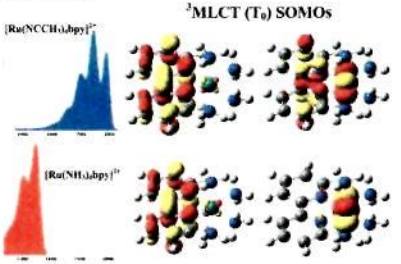

1199 dx.doi.org/10.1021/ic301181b

Improved Photochromic Properties on Viologen-Based Inorganic–Organic Hybrids by Using π-Conjugated Substituents as Electron Donors and Stabilizers

Rong-Guang Lin, Gang Xu, Ming-Sheng Wang, Gang Lu, Pei-Xin Li, and Guo-Cong Guo*

A series of asymmetric viologen chlorobismuthate hybrids have been synthesized for the first time. Studies on the relationship between the structure and photochromic behavior in this work clearly reveal that π-conjugated substituents could be used to improve the photoresponsibility and enrich the developed color efficiently and that the π···π interaction among organic components may not only be a powerful factor to stabilize the viologen monocation radical but also act as the second path of electron transfer from the π-conjugated substituent to the viologen cation for the photochromic process.

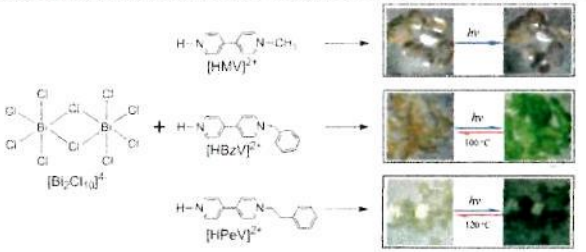

1206 dx.doi.org/10.1021/ic301440k

Synthesis and Properties of New Phosphorescent Red Light-Excitable Platinum(II) and Palladium(II) Complexes with Schiff Bases for Oxygen Sensing and Triplet–Triplet Annihilation-Based Upconversion

Sergey M. Borisov,* Robert Saf, Roland Fischer, and Ingo Klimant

New Pt(II) and Pd(II) complexes with Schiff bases show efficient absorption in the orange–red part of the spectrum and room-temperature near-infrared (NIR) phosphorescence. They are applied as indicators in optical oxygen sensors and as sensitizers in triplet–triplet annihilation-based upconversion systems.

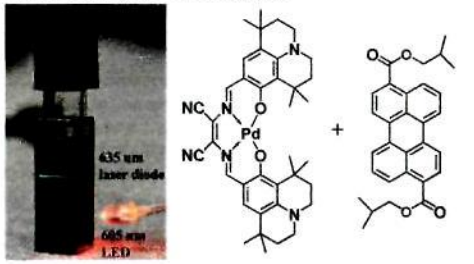

1217 dx.doi.org/10.1021/ic301512c

Quantum Chemical Topology Study of the Water-Platinum(II) Interaction

Jacqueline Bergès,* Isabelle Fourré, Julien Pilmé, and Jiri Kozelka

Beyond the stabilization energy, three topological descriptors characterize the nature of the non-conventional H-bonding of the complex-axial water interaction: one is the ELF localization domain of *cis*-$[PtCl_2(NH_3)_2]\cdot H_2O$ showing the deformation of the approaching OH bond.

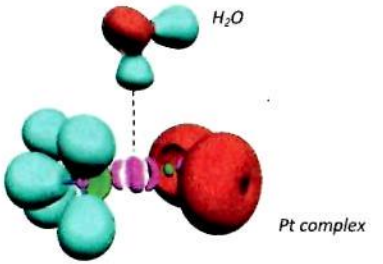

1228 dx.doi.org/10.1021/ic301530t

Computational Quantification of the Physicochemical Effects of Heme Distortion: Redox Control in the Reaction Center Cytochrome Subunit of *Blastochloris viridis*

Stuart A. MacGowan and Mathias O. Senge*

A facile, experimentally calibrated computational procedure is described that affords the relative ordering of heme cofactor reduction potentials with respect to intrinsic shifts brought about by apoprotein induced heme-macrocycle distortion. This technique was applied to the reaction center tetraheme cytochrome subunit of *Blastochloris viridis* and it was found that conformational control may account for up to 70% (54 mV) of the observed variation in the reduction potentials of the four hemes.

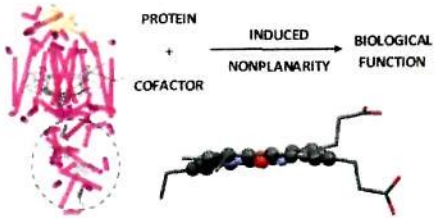

1238 dx.doi.org/10.1021/ic301609t

Synthetic, Crystallographic, and Computational Study of Copper(II) Complexes of Ethylenediaminetetracarboxylate Ligands

Zoran D. Matović,* Vesna D. Miletić, Marina Ćendić, Auke Meetsma, Petra J. van Koningsbruggen, and Robert J. Deeth*

Two novel complexes complete a series of copper(II) ethylenediaminetetracarboxylate chelates with n acetato and $4n$ β-propionato arms, where $n = 0-4$. The geometrical and electronic structures are examined in detail via single-crystal X-ray diffraction, electronic and IR spectroscopy, and theoretical calculations. Several relationships are established including a linear correlation between tetragonality and the number of five-membered rings in the complex anion and between tetragonality and the energy of the most intense d−d absorption. Ligand design features are presented that may aid the development of selective chelates for treating illnesses such as Wilson's disease.

1248 dx.doi.org/10.1021/ic301632y

Effects of Sequence, Connectivity, and Counter Ions in New Amide-Linked Ru(tpy)$_2$−Re(bpy) Chromophores on Redox Chemistry and Photophysics

Jan Dietrich, Ute Thorenz, Christoph Förster, and Katja Heinze*

Bimetallic Ru~Re complexes **1**−**3** were prepared from cationic metallo ligands **L1**−**L3** based on bis(terpyridine) ruthenium(II) complexes decorated with differently substituted 2,2′-bipyridines attached via amide groups. Counter ions or water molecules coordinate to the linking amide unit. The amide orientation, the connecting site at the bpy unit, and the coordination of counterions to the amide are shown to determine redox and photophysical properties of these multifunctional systems.

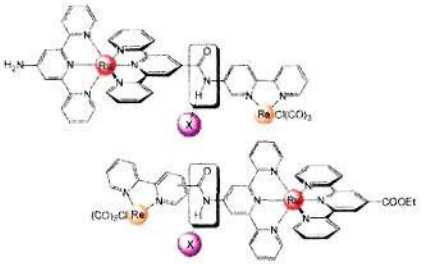

1265 dx.doi.org/10.1021/ic3017694

Large Oxygen Nonstoichiometry in $La_{0.77}Sr_{3.23}Co_{2.75}C_{0.25}O_{8.40+\delta}$ Oxide ($\delta = 0$, 1.3) Related to $n = 3$ RP Series

A. Demont, S. Hébert, J. Höwing, Y. Bréard, and D. Pelloquin*

Ruddlesden−Popper phase, $La_{0.77}Sr_{3.23}Co_{2.75}C_{0.25}O_{8.40+\delta}$ is an original Ruddlesden−Popper system that displays crystal chemistry comparable to cobalt perovskite materials. It shows a wide range of oxygen nonstoichiometry, yielding in a large variety of cobalt species formal oxidation states ranging from Co^{2+}/Co^{3+} when as synthesized to Co^{3+}/Co^{4+} when annealed under oxygen pressure. The potential richness deriving from this flexibility is illustrated in terms of magnetotransport properties and includes a resistivity that varies within a range of 5 orders of magnitude after modulation of the oxygen content with the appearance of negative magnetoresistance and ferromagnetic interactions due to Co^{3+}/Co^{4+} mixed-valence state.

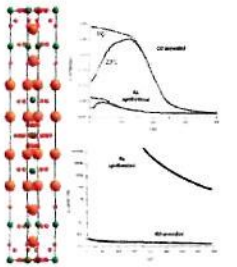

1275 dx.doi.org/10.1021/ic301794r

Isolation and Crystallographic Characterization of Sm@C_{2v}(3)-C_{80} Through Cocrystal Formation with Ni^{II}(octaethylporphyrin) or Bis(ethylenedithio)tetrathiafulvalene

Hua Yang, Zhimin Wang, Hongxiao Jin, Bo Hong, Ziyang Liu,* Christine M. Beavers, Marilyn M. Olmstead,* and Alan L. Balch*

Purified Sm@C_{2v}(3)-C_{80} has been isolated from the carbon soot produced by electrical arc vaporization of graphite rods doped with Sm_2O_3. Its structure has been determined by X-ray diffraction using cocrystals obtained from either Ni^{II}(octaethylporphyrin) (Ni^{II}(OEP)) to form Sm@C_{2v}(3)-C_{80}·Ni^{II}(OEP)·1.68(toluene)·0.32(benzene) or bis(ethylenedithio)-tetrathiafulvalene (ET) to produce Sm@C_{2v}(3)-C_{80}·ET·0.5-(toluene).

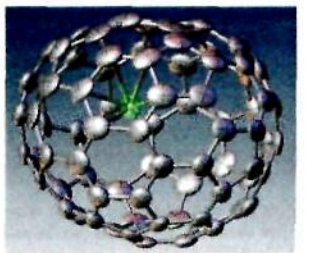

1285 S dx.doi.org/10.1021/ic301805y

Electron Spin Density on the Axial His Ligand of High-Spin and Low-Spin Nitrophorin 2 Probed by Heteronuclear NMR Spectroscopy

Luciano A. Abriata, María-Eugenia Zaballa, Robert E. Berry, Fei Yang, Hongjun Zhang, F. Ann Walker,* and Alejandro J. Vila*

We herein report the assignment of the ^{1}H, ^{13}C and ^{15}N resonances of the axial His ligand in the NO-carrying protein nitrophorin 2 in the paramagnetic high-spin and low-spin forms, and in the diamagnetic NO complex. Our work allowed us to map the electron spin density on both paramagnetic forms and describe how spin delocalization takes place, representing the deepest investigation available to date about the electronic structure of an axial heme ligand.

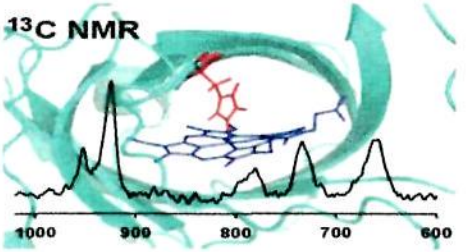

1296 S dx.doi.org/10.1021/ic301820w

Turning on Single-Molecule Magnet Behavior in a Linear {Mn_3} Compound

Fatemah Habib, Gabriel Brunet, Francis Loiseau, Thushan Pathmalingam, Tara J. Burchell, André M. Beauchemin, Wolfgang Wernsdorfer, Rodolphe Clérac,* and Muralee Murugesu*

The synthesis, structure, and magnetic properties are reported for a new manganese compound with a mixed-valent {Mn_3} core arranged in a linear fashion. The structure reveals Mn^{IV}–Mn^{III}–Mn^{IV} units connected through Na^{+} ions forming a linear one-dimensional coordination polymer. Magnetic susceptibility measurements reveal single-molecule magnet behavior due to the anisotropy introduced by the Jahn–Teller distortions on the Mn^{III} ions.

1304 S dx.doi.org/10.1021/ic3018387

Synthesis, Characterization, and Photophysics of Oxadiazole- and Diphenylaniline-Substituted Re(I) and Cu(I) Complexes

Raphael Horvath, Michael G. Fraser, Scott A. Cameron, Allan G. Blackman, Pawel Wagner, David L. Officer, and Keith C. Gordon*

Oxadiazole and diphenyl aniline-substituted 2,2′-bipyridyl–rhenium(I) and –copper(I) complexes have been synthesized and characterized using crystallography, resonance Raman, time-resolved absorption and emission spectroscopies, and density functional theory. The optical properties of the oxadiazole complexes are MLCT in nature, and the lowest excited state is ^{3}MLCT. For complexes with the diphenyl aniline substituents the optical properties are dominated by the ligand; the lowest excited state is an intraligand charge transfer state (^{3}ILCT).

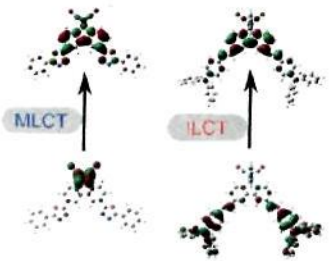

1318 S dx.doi.org/10.1021/ic301865n

Ligand-Field and Ligand-Binding Analysis of the Active Site of Copper-Bound Aβ Associated with Alzheimer's Disease

Chandradeep Ghosh and Somdatta Ghosh Dey*

Cu-Aβ has two components at physiological pH that are in equilibrium with a pK_a of ~8.1. Ligand-field analysis indicates five-coordinate geometry for both components. Exogenous ligand binding to the active site indicates the presence of a water-derived ligand and a second exchangeable ligand, likely a backbone amide carbonyl, occupying the equatorial plane of a square-pyramidal-type active-site geometry.

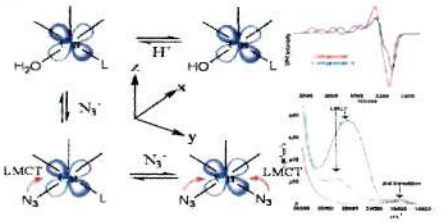

1328 S dx.doi.org/10.1021/ic301933a

Rhombohedrally Distorted γ-$Au_{5-x}Zn_{8+y}$ Phases in the Au–Zn System

Srinivasa Thimmaiah* and Gordon J. Miller

Reinvestigation of the γ region of the Au–Zn phase diagram revealed that the γ-$Au_{5-x}Zn_{8+y}$ phases adopt a rhombohedrally distorted Cr_5Al_8-type rather than a cubic Cu_5Zn_8-type structure. Single-crystal structural refinements showed the presence of vacancies on the Au sites, which reduces the overall valence-electron concentration to optimal values required for the stability of γ phases, i.e., between 1.61 and 1.66 electrons/atom.

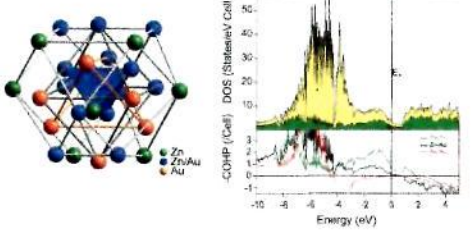

1338 S dx.doi.org/10.1021/ic302031f

Mechanisms for the Reactions of Group 10 Transition Metal Complexes with Metal–Group 14 Element Bonds, Bbt(Br)E=M(PCy_3)$_2$ (E = C, Si, Ge, Sn, Pb; M = Pd and Pt)

Wei-Hung Liao, Pei-Yun Ho, and Ming-Der Su*

The B3LYP computational results suggest that the relative chemical reactivity of Bbt(Br)E=M(PCy_3)$_2$ (E = C, Si, Ge, Sn, Pb and M = Pd, Pt) species decreases in the order, C=M > Si=M > Ge=M > Sn=M > Pb=M, irrespective of whether Pd or Pt is chosen. That is, the heavier the group 14 atom E involved, the more stable are its doubly bonded Bbt(Br)E=M(PCy_3)$_2$ compounds toward formation reactions and water additions.

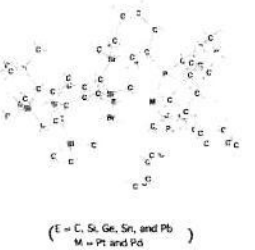

1349 dx.doi.org/10.1021/ic3020332

Intense Turquoise and Green Colors in Brownmillerite-Type Oxides Based on Mn^{5+} in $Ba_2In_{2-x}Mn_xO_{5+x}$

*Peng Jiang, Jun Li, A. Ozarowski, Arthur W. Sleight, and M. A. Subramanian**

Brownmillerite-type oxides $Ba_2In_{2-x}Mn_xO_{5+x}$ ($x = 0.1-0.7$) have been prepared and characterized. Magnetic measurements indicate that manganese in as-prepared samples is substituting predominantly as Mn^{5+} for all values of x with observed paramagnetic spin-only moments close to values expected for two unpaired electrons.

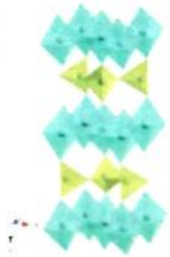

1358 dx.doi.org/10.1021/ic302050m

Copper(I)-α-Synuclein Interaction: Structural Description of Two Independent and Competing Metal Binding Sites

Francesca Camponeschi, Daniela Valensin,* Isabella Tessari, Luigi Bubacco, Simone Dell'Acqua, Luigi Casella, Enrico Monzani, Elena Gaggelli, and Gianni Valensin

In this work, the interaction of α-synuclein (αS) with Cu^I has been investigated by means of NMR and circular dichroism analysis on the full-length protein (αS_{1-140}) and on two, designed *ad hoc*, model peptides: αS_{1-15} and $\alpha S_{113-130}$. In addition to Cu^I, Ag^I has been used as a probe for Cu^I binding to αS_{1-140}. Two distinct Cu^I/Ag^I binding domains with comparable affinities, involving Met-1, Met-5 and Met-116, Met-127 residues, have been identified and extensively characterized.

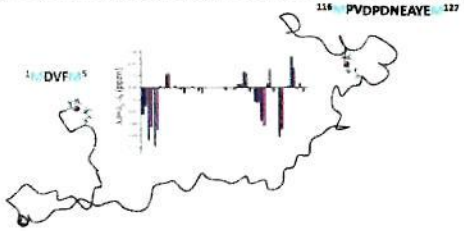

1368 dx.doi.org/10.1021/ic302055r

Syntheses and Photophysical Investigations of Cr(III) Hexadentate Iminopyridine Complexes and Their Tris(Bidentate) Analogues

Ashley M. McDaniel, Huan-Wei Tseng, Ethan A. Hill, Niels H. Damrauer, Anthony K. Rappé, and Matthew P. Shores*

Tripodal hexadentate and tris(bidentate) Cr(III) complexes based on iminopyridine ligands show similar ground state structural, electrochemical, and spectroscopic properties, and improved visible spectrum absorption relative to aromatic diimine congeners. However, excited state properties are surprisingly different for the iminopyridine complexes, where addition of a ligand tether turns off ^2E emission. Extensive computational analyses provide insight into this phenomenon.

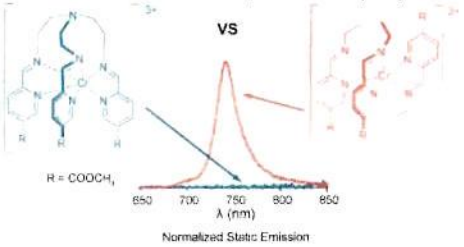

1379 dx.doi.org/10.1021/ic302063u

Luminescent Zinc(II) Complexes of Fluorinated Benzothiazol-2-yl Substituted Phenoxide and Enolate Ligands

Zhe Li, Ahmed Dellali, Jahangir Malik, Majid Motevalli, Roger M. Nix, Toyin Olukoya, Yu Peng, Huanqing Ye, William P. Gillin, Ignacio Hernández, and Peter B. Wyatt*

Fluorinated analogs of the important dinuclear photo- and electroluminescent material $[Zn(BTZ)_2]_2$, where H-BTZ = 2-(2-hydroxyphenyl)benzothiazole, are found to be mononuclear. They easily sublime and show broad, bright visible photoluminescence emission spectra. DFT calculations indicate that HOMO and LUMO energy levels in these materials are substantially lowered by fluorination.

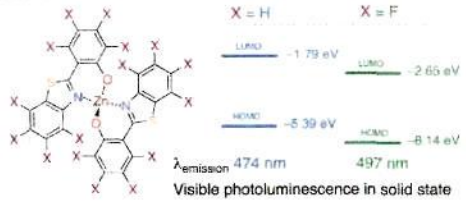

1388 dx.doi.org/10.1021/ic3020942

Bifunctional Mesoporous Zirconium Phosphonates for Delivery of Nucleic Acids

Yan Tang, Yubao Ren, and Xin Shi*

Bifunctional mesoporous zirconium phosphonates (ZrBFs) have been designed for oral delivery of nucleic acids through simultaneously integrating two different phosphonic acids into the frameworks wherein l-proline groups and piperazine groups endow the materials with pH-controllable release function (pH sensitivity) and high cell penetration capability (functionalizability). By dip-coating lag-time films on pH-sensitive ZrBFs loading nucleic acids, the time- and pH-controlled oral colon-targeted nucleic acid delivery systems have been developed, which can effectively protect nucleic acids with the intact in acidic medium of the stomach and efficiently deliver nucleic acids to the colon. Delivery of nucleic acids in such a way could improve delivery efficiency, bioactivity conservation, and bioavailability of nucleic acid through dual-controlled release, lag-time films coating, and further functionalization with cell-penetrating peptides, respectively.

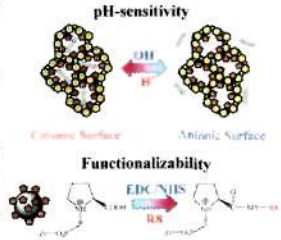

1398 dx.doi.org/10.1021/ic302095h

Lanthanide Dinuclear Complexes Involving Tetrathiafulvalene-3-pyridine-N-oxide Ligand: Semiconductor Radical Salt, Magnetic, and Photophysical Studies

Fabrice Pointillart,* Boris Le Guennic, Olivier Maury, Stéphane Golhen, Olivier Cador, and Lahcène Ouahab

Irradiation of the charge transfer bands of the $[Nd(tta)_3(L)]_2$ dinuclear complex provokes the Nd^{III} luminescence. The sensitization process may include a photoinduced electron transfer from the $^1TTF^*$ to the acceptor to generate the separated-charge $[TTF^{\bullet+}-3\text{-Py-}N\text{-oxide}^{\bullet-}\{Nd(tta)_3\}]$ state. Then, back-electron transfer occurs, and the Nd^{III} centers are sensitized by energy transfer.

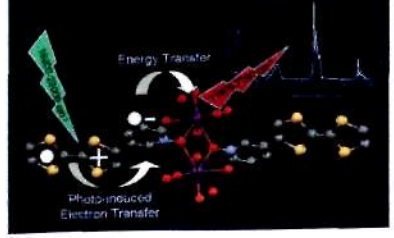

1409 dx.doi.org/10.1021/ic302128q

π-Bonded Dithiolene Complexes: Synthesis, Molecular Structures, Electrochemical Behavior, and Density Functional Theory Calculations

Aurélie Damas, Lise-Marie Chamoreau, Andrew L. Cooksy, Anny Jutand,* and Hani Amouri*

The π-bonded dithiolene complex **2**, isolated for the first time, reacts with the organometallic solvated species $[Cp^*M(acetone)_3][OTf]_2$ (M = Rh, Ir) to give a unique class of binuclear dithiolene compounds $[Cp^*Ir(C_6H_4S_2)MCp^*][OTf]_2$ [M = Rh (**3**), Ir (**4**)]. The electrochemical behavior of all complexes is investigated as well as density functional theory (DFT) and time-dependent DFT calculations. The presence of Cp*M at the arene system of the dithiolene ligand increases the stability compared to the known mononuclear species $[Cp^*Ir\text{-}o\text{-}(C_6H_4S_2\text{-}\kappa^2\text{-}S,S)]$ and enables the complexes $Cp^*Ir(C_6H_4S_2)MCp^*][OTf]_2$ (**3** and **4**) to act as electron reservoirs.

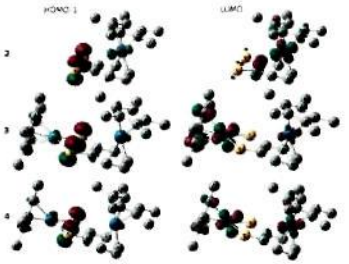

1418 dx.doi.org/10.1021/ic302148s

Pressure-Dependent Increase in T_c and Magnetic Behavior of $[Ru_2(O_2CBu^t)_4]_3[M(CN)_6]\cdot 2H_2O$ (M = Cr, Fe)

Jack G. DaSilva and Joel S. Miller*

Magnetization as a function of applied pressure up to 10.16 kbar and magnetic field were obtained for layered $[Ru_2(O_2CBu^t)_4]_3[M(CN)_6]\cdot 2H_2O$ (M = Cr, Fe). For M = Fe, the T_c increased by 13% from 6.1 to 6.9 K with a significant increase in the coercive field, H_{cr}, from 5 to 65 Oe, followed by a sharp decrease to less than 10 Oe at further applied pressure.

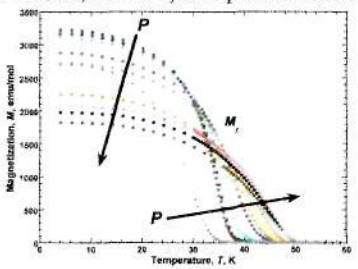

1424 dx.doi.org/10.1021/ic302153s

Synthesis and Structural Characterization of Heteroboroxines with MB_2O_3 Core (M = Sb, Bi, Sn)

Barbora Mairychová, Tomáš Svoboda, Petr Štěpnička, Aleš Růžička, Remco W. A. Havenith, Mercedes Alonso, Frank De Proft,* Roman Jambor,* and Libor Dostál*

Novel heteroboroxines containing the MB_2O_3 (M = Sb, Bi, Sn) core were prepared by straightforward high-yielding procedures. The heteroatoms present within these nonaromatic ring systems are stabilized by coordination of an NCN pincer-type ligand.

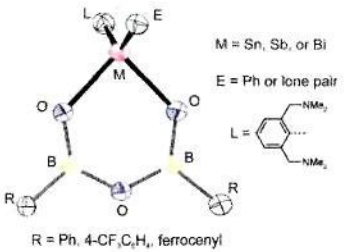

1432 dx.doi.org/10.1021/ic302155e

Reactions of Acids with Naphthyridine-Functionalized Ferrocenes: Protonation and Metal Extrusion

Nabanita Sadhukhan, Mithun Sarkar, Tapas Ghatak, S. M. Wahidur Rahaman, Leonard J. Barbour, and Jitendra K. Bera*

Reactions of certain protonic acids with naphthyridyl-ferrocene FcNP causes partial demetalation affording a variety of Fe complexes. The amount of the acid, the reaction time, and the coordinating ability of the conjugate base influence the metal extrusion and the product identity as well. Acid-mediated demetalation occurs only for monosubstituted ferrocene FcNP whereas bis-substituted $FcNP_2$ affords protonated products.

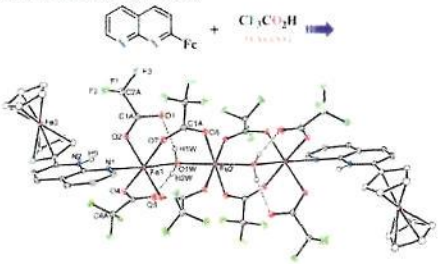

1443 dx.doi.org/10.1021/ic3021782

Second Sphere Control of Redox Catalysis: Selective Reduction of O_2 to O_2^- or H_2O by an Iron Porphyrin Catalyst

Subhra Samanta, Kaustuv Mittra, Kushal Sengupta, Sudipta Chatterjee, and Abhishek Dey*

An iron porphyrin complex bearing four ferrocene groups is found to bind O_2 and quantitatively reduce it by one electron to O_2^- in apolar organic solvents and by four electrons to H_2O in an aqueous medium. This selectivity of O_2 reduction is governed by the reduction potential of the distal ferrocene groups which depends on the solvent.

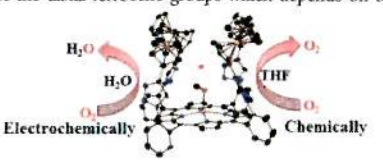

1454 dx.doi.org/10.1021/ic3021904

Unexpected Formation of Chiral Pincer CNN Nickel Complexes with β-Diketiminato Type Ligands via C−H Activation: *Synthesis, Properties, Structures, and Computational Studies*

Zhengliang Lu, Srinivas Abbina, Jared R. Sabin, Victor N. Nemykin,* and Guodong Du*

A series of unsymmetrical and chiral CNN pincer nickel complexes with C_1 symmetric, β-diketimine type ligands, formed via an unexpected benzylic and aryl C−H bond activation, have been described.

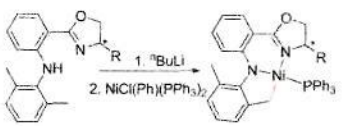

1466 dx.doi.org/10.1021/ic302205b

Phosphido-Borane and Phosphido-Bis(Borane) Complexes of the Alkali Metals, a Comparative Study

Keith Izod,* James M. Watson, William Clegg, and Ross W. Harrington

While they are isoelectronic analogues of silyl ligands and silanes, phosphido-borane $[R_2P(BH_3)]^-$ and phosphido-bis(borane) $[R_2P(BH_3)_2]^-$ ligands have received little attention; the present study shows that these ligands adopt a variety of coordination modes in their complexes with the alkali metals, although these are dominated by B−H···M contacts.

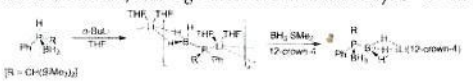

1476 dx.doi.org/10.1021/ic302218m

Tuning of "Antenna Effect" of Eu(III) in Ternary Systems in Aqueous Medium through Binding with Protein

Shyamal Kr Ghorai, Swarna Kamal Samanta, Manini Mukherjee, Pinki Saha Sardar, and Sanjib Ghosh*

Ternary system consisting of a protein (serum albumins), tetracycline (TC), and Eu(III) exhibits very efficient "antenna effect" in aqueous medium. The highly efficient sensitization from TC and subsequent efficient shielding of the $^5D_0$ state of Eu(III) from the O−H oscillator provided by the interior binding site of the proteins are responsible for this effect. In the *E. coli* alkaline phosphatase−TC−Eu(III) system, the binding of TC at the surface of the protein leads to inefficient "antenna effect".

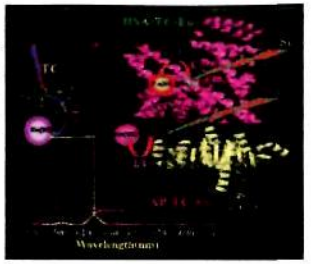

1488 dx.doi.org/10.1021/ic302246c

New Molybdenum(VI) Phosphates: Synthesis, Characterization, and Calculations of Centrosymmetric $RbMoO_2PO_4$ and Noncentrosymmetric $Rb_4Mo_5P_2O_{22}$

Ying Wang, Shilie Pan,* Xin Su, Zhihua Yang,* Lingyun Dong, and Min Zhang

Two new molybdenum(VI) phosphates, $RbMoO_2PO_4$ and $Rb_4Mo_5P_2O_{22}$, have been synthesized by a standard solid-state reaction. $RbMoO_2PO_4$ is centrosymmetric with a three-dimensional framework structure related to gismondine (GIS), whereas $Rb_4Mo_5P_2O_{22}$ is noncentrosymmetric with a one-dimensional chain structure consisting of Strandberg-type units. Powder second-harmonic generation (SHG) measurements on $Rb_4Mo_5P_2O_{22}$ indicate that the material has an SHG efficiency ~ 1.4 times that of KH_2PO_4.

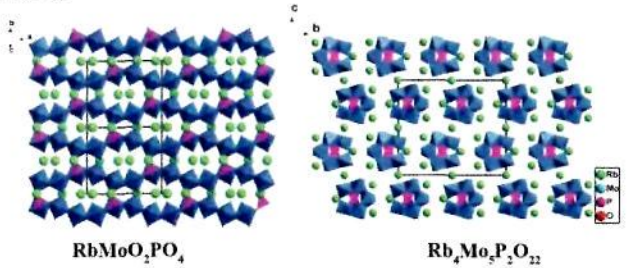

1496 dx.doi.org/10.1021/ic3022535

Synthesis of Small Tetranuclear Cu(I) Metallacycles Based on Bridging Pseudohalogenide Ions

Volodymyr Vreshch, Brigitte Nohra, Christophe Lescop,* and Régis Réau*

Reactions of pseudohalide ions acting as 'short' linkers with 'U-shape' Cu^I bimetallic molecular clips bearing short intermetallic distances afforded selectively tetrametallic metallacycles, including a nitrogen-rich Cu_2N_6 ring, rather than coordination polymers. The formation of the metallacycles can be explained by the steric hindrance of the bulky N,P,N-ligands bearing a bridging phosphole used to stabilize the Cu^I bimetallic clip.

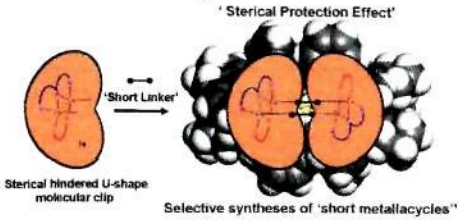

1504 dx.doi.org/10.1021/ic302258k

Role of Substitution at Terminal Nitrogen of 2-Oxo-1,2-dihydroquinoline-3-Carbaldehyde Thiosemicarbazones on the Coordination Behavior and Structure and Biological Properties of Their Palladium(II) Complexes

Eswaran Ramachandran, Duraisamy Senthil Raja, Nigam. P. Rath, and Karuppannan Natarajan*

The influence of monosubstitution at the terminal nitrogen of 2-oxo-1,2-dihydroquinoline-3-carbaldehyde thiosemicarbazone on the structures and in vitro pharmacological properties of mixed ligand Pd(II) complexes has been evaluated and reported in this paper. The overall investigations strongly support that the terminal N substitution in thiosemicarbazone has affected not only the structure and the nature of the complexes but also the various pharmacological properties of the resulting Pd(II) complexes.

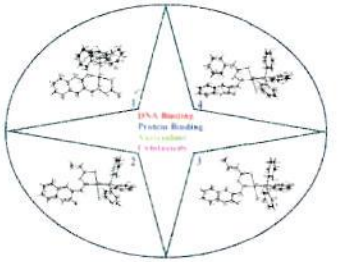

1515 dx.doi.org/10.1021/ic302268h

Molecular Structure, UV/Vis Spectra, and Cyclic Voltammograms of Mn(II), Co(II), and Zn(II) 5,10,15,20-Tetraphenyl-21-oxaporphyrins

Silvio Stute, Linda Götzke, Dirk Meyer, Mohamed L. Merroun, Peter Rapta, Olga Kataeva, Wilhelm Seichter, Kerstin Gloe, Lothar Dunsch, and Karsten Gloe*

The 5,10,15,20-tetraphenyl-21-oxaporphyrin complexes of Mn(II), Co(II), Cu(II), and Zn(II) have been crystallized and characterized by X-ray diffraction, NMR and UV/vis spectroscopy, mass spectrometry, and cyclic voltammetry. The crystal structures show square pyramidal coordination geometries having chloride in the axial position for all four complexes. In case of Zn(II) the octahedral coordination sphere could be realized by an oxaporphyrin having a flexible side chain with an OH donor function.

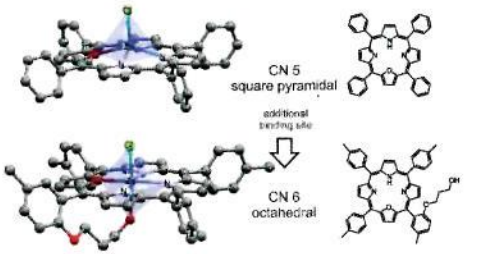

1525 S dx.doi.org/10.1021/ic302278q

Low-Dimensional 3d–4f Complexes Assembled by Low-Spin $[Fe^{III}(phen)(CN)_4]^-$ Anions

Diana Visinescu,* Luminita Marilena Toma, Oscar Fabelo, Catalina Ruiz-Pérez, Francesc Lloret, and Miguel Julve*

New low-dimensional cyanide and bpym bridged $\{Fe^{III}Ln^{III}\}$ heterobimetallic complexes have been obtained by reacting the six-coordinate $[Fe^{III}(phen)(CN)_4]^-$ anions with partially blocked $[Ln(bpym)(H_2O)_x(NO_3)]^{3+}$ cationic complexes [Ln^{III} = Gd (**1**), Tb (**2**), Sm (**3**), and Pr (**4**)]. Compounds **1**–**3** are isomorphous with a ladder-like structure, while **4** exhibits a unique layered structure. Weak antiferro- and ferromagnetic magnetic interactions were observed for compounds **1** and **3**, respectively.

1538 S dx.doi.org/10.1021/ic302333e

The First Vanadate–Carbonate, $K_2Mn_3(VO_4)_2(CO_3)$: Crystal Structure and Physical Properties

Olga V. Yakubovich, Ekaterina V. Yakovleva, Alexey N. Golovanov, Anatoly S. Volkov, Olga S. Volkova, Elena A. Zvereva, Olga V. Dimitrova, and Alexander N. Vasiliev*

The potassium manganese vanadate–carbonate, $K_2Mn_3(VO_4)_2(CO_3)$, representing a novel structure type, has been synthesized hydrothermally in the system $MnCl_2$–K_2CO_3–V_2O_5–H_2O. The title compound exhibits rich physical properties reflected in a phase transition of presumably Jahn–Teller origin at T_3 = 80–100 K and two successive magnetic phase transitions at T_2 = 3 K and T_1 = 2 K into a weakly ferromagnetic ground state.

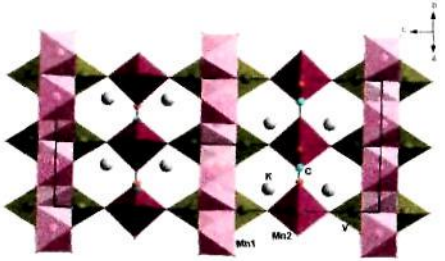

1544 S dx.doi.org/10.1021/ic302344a

Oxidative Addition Versus Substitution Reactions of Group 14 Dialkylamino Metalylenes with Pentafluoropyridine

Prinson P. Samuel, Amit Pratap Singh, Sankaranarayana Pillai Sarish, Julia Matussek, Ina Objartel, Herbert W. Roesky,* and Dietmar Stalke*

Pentafluoropyridine undergoes oxidative addition reaction at the amino functionalized Ge(II) center depicting the C–F bond activation by the lone pair of a germanium atom. A similar reaction using the amino functionalized Sn(II) renders the substitution reaction affording the Sn(II) fluoride compound, a promising mild fluorinating agent.

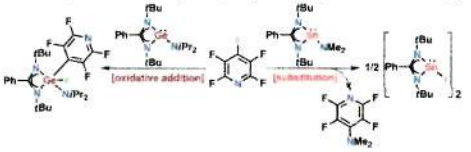

1550 dx.doi.org/10.1021/ic302346g

Structural Transformations and Disordering in Zirconolite ($CaZrTi_2O_7$) at High Pressure

Ashkan Salamat,* Paul F. McMillan,* Steven Firth, Katherine Woodhead, Andrew L. Hector, Gaston Garbarino, Martin C. Stennett, and Neil C. Hyatt

There is interest in identifying novel materials for use in radioactive waste applications and studying their behavior under high pressure conditions The mineral zirconolite ($CaZrTi_2O_7$) has been identified as a potential ceramic phase for radionuclide sequestration. In this study, we probed the high pressure structural properties of this pyrochlore-like structure to study its phase transformations and possible amorphization behavior. Combined synchrotron X-ray diffraction and Raman spectroscopy studies reveal a series of high pressure phase transformations.

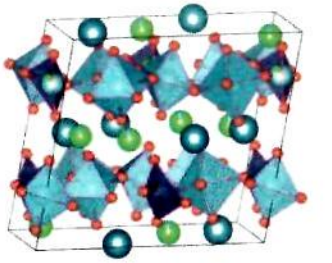

1559 S dx.doi.org/10.1021/ic302378r

Iron(III) Complexes with Meridional Ligands as Functional Models of Intradiol-Cleaving Catechol Dioxygenases

Tünde Váradi, József S. Pap, Michel Giorgi, László Párkányi, Tamás Csay, Gábor Speier, and József Kaizer*

Adducts of 3,5-di-*tert*-butylcatechol with the Fe(III) complexes of meridional isoindoline-based ligands react with dioxygen yielding ring-cleaved products with high intradiol over extradiol selectivity. Kinetic measurements in combination with electrochemical investigations revealed an inverse trend between reaction rates and oxidation potentials associated with the coordinated catecholate. On the basis of these results, a substrate activation mechanism is suggested for this system in which the geometry of the peroxide-bridged intermediate may be of key importance in regioselectivity.

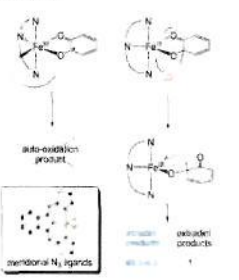

1570 S dx.doi.org/10.1021/ic302449n

Base-Induced Dehydrogenation of Ruthenium Hydrazine Complexes

Leslie D. Field,* Hsiu L. Li, Scott J. Dalgarno, and Ruaraidh D. McIntosh

A series of side-on bound hydrazine, phenylhydrazine, and methylhydrazine complexes have been synthesized on Ru containing the tripodal phosphine ligand PP_3^{iPr} while the analogous complexes with PP_3^{Ph} contain end-on bound hydrazine ligands. Base treatment of the hydrazine complexes afforded a range of products including the dinitrogen and dihydride complexes as well as a hydrido ruthenaindazole complex and a hydrido methylenehydrazide complex.

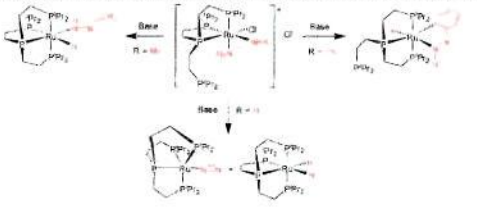

1584 S dx.doi.org/10.1021/ic302455y

Isolable, Copper(I) Dicarbonyl Complexes Supported by *N*-Heterocyclic Carbenes

Chandrakanta Dash, Animesh Das, Muhammed Yousufuddin, and H. V. Rasika Dias*

N-Heterocyclic carbenes are capable of stabilizing copper(I) dicarbonyls.

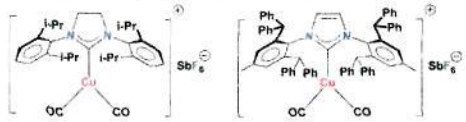

1591 S dx.doi.org/10.1021/ic302460y

Structural and Spectroscopic Characterization of 17- and 18-Electron Piano-Stool Complexes of Chromium. Thermochemical Analyses of Weak Cr−H Bonds

Edwin F. van der Eide, Monte L. Helm, Eric D. Walter, and R. Morris Bullock*

The reaction of N-heterocyclic carbene 1,3-dimethylimidazol-2-ylidene (IMe) with $[CpCr(CO)_3]_2$ gives the 17-electron $CpCr(CO)_2(IMe)^{\bullet}$, which was fully characterized. Reduction with KC_8 provides $K^+[CpCr(CO)_2(IMe)]^-$, which was crystallographically characterized in the presence and in the absence of 18-crown-6. Hydride $CpCr(CO)_2(IMe)H$ was generated by protonation of $CpCr(CO)_2(IMe)^-$, and was spectroscopically characterized. The Cr−H bond dissociation free energy of $CpCr(CO)_2(IMe)H$ in MeCN is only 47.3(6) kcal mol^{-1}, making it among the weakest M-H bonds of any organometallic hydride.

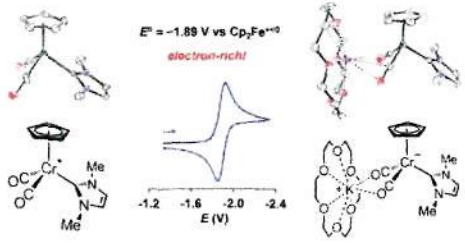

1604 S dx.doi.org/10.1021/ic3025155

Pd^{2+}-Incorporated Perovskite $CaPd_3B_4O_{12}$ (B = Ti, V)

Kentaro Shiro, Ikuya Yamada,* Naoya Ikeda, Kenya Ohgushi, Masaichiro Mizumaki, Ryoji Takahashi, Norimasa Nishiyama, Toru Inoue, and Tetsuo Irifune

Novel *A*-site ordered perovskites $CaPd_3Ti_4O_{12}$ and $CaPd_3V_4O_{12}$ were synthesized using a high-pressure synthesis method. These compounds are the first example in which a crystallographic site of a perovskite structure is entirely occupied by Pd^{2+} ions. $CaPd_3Ti_4O_{12}$ is a diamagnetic insulator whereas $CaPd_3V_4O_{12}$ is a Pauli-paramagnetic metal.

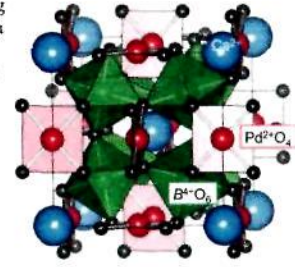

1610 S dx.doi.org/10.1021/ic302532f

High Nuclearity Complexes of Lanthanide Involving Tetrathiafulvalene Ligands: Structural, Magnetic, and PhotoPhysical Properties

Fabrice Pointillart,* Boris Le Guennic, Stéphane Golhen, Olivier Cador, Olivier Maury, and Lahcène Ouahab

Redox active paramagnetic tetranuclear complexes of formula $[Ln_4(hfac)_{12}(L)_2]$ have been obtained. Upon irradiation at 20835 cm^{-1}, both Er(III) and Yb(III) derivatives display a metal-centered luminescence respectively attributed to $^4I_{13/2} \rightarrow {}^4I_{15/2}$ (6660 cm^{-1}) and $^2F_{5/2} \rightarrow {}^2F_{7/2}$ (9970 cm^{-1}) excitations. The Yb(III) analogue has a $M_J = \pm 5/2$ ground state.

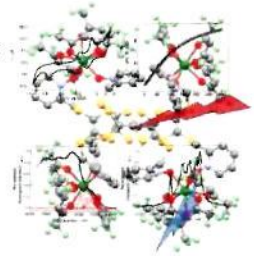

1621 S dx.doi.org/10.1021/ic302535h

Phenylcyanamidoruthenium Scorpionate Complexes

Carmen Harb, Pavel Kravtsov, Mohommad Choudhuri, Eric R. Sirianni, Glenn P. A. Yap, A. B. P. Lever,* and Robert J. Crutchley*

As shown by density functional theory calculations, oxidation of [Ru(Tp)(dppe)L], where Tp is hydrotris(pyrazol-1-yl)borate, dppe is ethylenebis(diphenylphosphine), and L is a substituted phenylcyanamide ligand, leads to species where partial oxidation of the cyanamide ligand has occurred, indicative of noninnocent character for these ligands. $[\{Ru(Tp)(dppe)\}_2(\mu\text{-adpc})]^+$, where $adpc^{2-}$ is azo-4,4-diphenylcyanamide, shows a vis/near-IR spectrum consistent with a delocalized mixed-valence state.

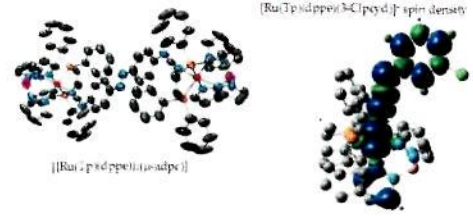

1631 S dx.doi.org/10.1021/ic302537d

Insight into One-Electron Oxidation of the $\{Fe(NO)_2\}^9$ Dinitrosyl Iron Complex (DNIC): Aminyl Radical Stabilized by $[Fe(NO)_2]$ Motif

Chih-Chin Tsou, Fu-Te Tsai, Huang-Yeh Chen, I-Jui Hsu, and Wen-Feng Liaw**

A reversible redox reaction $\{Fe(NO)_2\}^9$ DNIC $[(NO)_2Fe(N(Mes)(TMS))_2]^-$ ⇄ oxidized-form DNIC $[(NO)_2Fe(N(Mes)(TMS))_2]$ (a delocalized aminyl radical $[(N(Mes)(TMS))_2^{\bullet}]$ stabilized by the electron-deficient $\{Fe^{III}(NO^-)_2\}^9$ motif) was demonstrated (Mes = mesityl, TMS = trimethylsilane).